ACI STRUCTURAL JOURNAL TECHNICAL PAPER

Title no. 108-S27

Failure Mode Transitions in Reinforced Concrete Beams—Part 2: Experimental Tests

by Alberto Carpinteri, Jacinto Ruiz Carmona, and Giulio Ventura

This paper presents the results of an experimental research program validating a recently developed mechanical model connecting failure modes with cracking processes in reinforced concrete (RC) beams. In the analysis of the experimental results, special emphasis is given to the shape, extension, and initial location of the main tensile or shear crack and their relation to the rupture mode of the RC beam. The experimental program investigated five different reinforcement percentages with four samples each, for a total of 20 beams subjected to a three-point bending test. The experimental results are discussed with the help of the bridged crack model. The model unifies the theoretical treatment of yielding, shear, and crushing failures to predict collapse mode transitions and related size effects, and the experimental program is focused on validating and discussing the choice of some model parameters.

Keywords: brittle-to-ductile failure transition; critical crack; crushing failure; shear strength.

INTRODUCTION

During the loading process, several crack patterns may form in a reinforced concrete (RC) beam before beam collapse. The trajectory and extension of these cracks will define the kind of failure. For example, in three-point bending, the first crack would form in the region of maximum bending moment, where the maximum principal stress attains the material tensile strength. Recently, flexural cracks and flexural failure have been widely analyzed. Several experimental programs were undertaken, mainly on lightly reinforced beams, designed so that only one main flexural crack crosses the reinforcement layer and fracture mechanics can be conveniently applied to derive a mechanical model of the RC beam.[1-9] As the amount of reinforcement is increased, several cracks are formed along the beam. In the early stages, these cracks are approximately normal to the beam axis and, as cracking progresses, they grow in the presence of combined normal and shear stresses as mixed-mode flexural-shear cracks. If the reinforcement percentage is sufficiently high, usually one of the flexural-shear cracks suddenly propagates, unstably leading to the failure of the beam. This kind of collapse is known in the literature[10-12] as diagonal tension failure. The problem analyzed in this paper is finding a relation between the reinforcement percentage and the initial location and shape of the failure crack, determining the beam failure mode. Complementary transitions between failure modes may be drawn. The experimental program and mechanical model refer to RC beams without stirrups.

A series of 20 beams with five reinforcement percentages has been tested by three-point bending in displacement control and a quasi-static condition. The midspan force and displacements at seven different points have been measured (supports, midspan, and thirds of the half-span). Moreover, the failure crack path has been acquired by a digital camera and processed.

The first part of this paper focuses on the presentation of the experimental program, whereas the second part discusses the experimental results with reference to the bridged crack model.[1,13] This is of particular importance, as it completes and experimentally validates the theoretical model.[1,13]

RESEARCH SIGNIFICANCE

The problem analyzed in this paper is finding a relation between the failure mode and the initial location, shape, and extension of cracks. This study focuses on the analysis of the critical crack, representing the crack whose opening leads the beam to collapse. A comprehensive report of experimental data on this topic is unavailable in the literature, whereas these data are indispensable for the validation of mechanical models based on fracture mechanics theories. In particular, these data are presented herein and used in connection with the bridged crack model,[1] aimed at a rational explanation of the relation between cracking processes and beam collapse, including the relevant size effects.

OVERVIEW OF EXPERIMENTAL PROGRAM

The program was designed to study the influence of the reinforcement ratio on the crack pattern in RC beams. Although with increasing reinforcement ratios, concrete cracking spreads all over the beam, attention is devoted to the determination of initial location and shape of the crack whose opening finally determines the beam failure (critical crack) in relation to the reinforcement percentage.

To examine all the most significant failure modes (yielding, shear, and crushing), the design of the RC beams was conditioned by the following requirements:

1. The lowest reinforcement ratio had to correspond to the minimum mechanical reinforcement percentage;
2. The next reinforcement ratio had to correspond to a beam with a failure mode close to the transition between flexural and shear failure;
3. A third reinforcement ratio had to represent a shear failure (diagonal tension failure); and
4. The highest reinforcement ratio had to induce concrete crushing failure in the top part of the beam.

For model calibration, unreinforced beams were considered as well, giving a total of five reinforcement percentages.

ACI Structural Journal, V. 108, No. 3, May-June 2011.
MS No. S-2008-359.R1 received April 1, 2010, and reviewed under Institute publication policies. Pertinent discussion including author's closure, if any, will be published in the March-April 2012 *ACI Structural Journal* if the discussion is received by November 1, 2011.

Alberto Carpinteri *has been a Full Professor of structural mechanics at the Politecnico di Torino, Torino, Italy, since 1986. He received doctoral degrees in nuclear engineering and mathematics from the University of Bologna, Bologna, Italy, in 1976 and 1981, respectively.*

Jacinto Ruiz Carmona *is a Research Assistant in solid mechanics and materials science at the University of Castilla-La Mancha (UCLM), Castilla-La Mancha, Spain. He received his degree in civil engineering from Madrid Polytechnical University, Madrid, Spain, and his PhD in solid mechanics from UCLM in 2000 and 2006, respectively. His research interests include the fracture of plain and reinforced concrete.*

Giulio Ventura *is an Associate Professor of structural mechanics at the Politecnico di Torino. He received his MS in civil engineering and his PhD in structural engineering from the University of Catania, Catania, Italy, in 1990 and 1994, respectively. His research interests include computational mechanics and reinforced concrete theoretical and experimental research.*

The beam geometry, test arrangement, and steel reinforcement are reported in Fig. 1. The dimensions of the samples were chosen for easy laboratory handling and the longitudinal steel reinforcement, arranged with a constant cover of 0.47 in. (12 mm), is uniform over the entire length of the beam. The distance between supports is equal to six times the depth of the beam.

Figure 1(b) sketches the central cross section of the beams for the considered longitudinal reinforcement. Each specimen is then named after the nominal diameter of the reinforcing bars in millimeters. The reinforcement percentage corresponding to each sample is reported within parentheses.

Materials characterization was obtained by independent tests performed according to standard recommendations. The compressive strength, elastic modulus, and fracture energy were determined for the concrete, and the yield and ultimate strength for the steel reinforcing bars were obtained from the tensile tests.

Details of the characterization program are presented in the following section. All the tests were carried out at the Department of Structural and Geotechnical Engineering at the Politecnico di Torino.

MATERIALS TESTING

A single concrete mixture was used throughout the experimental program. The specimen-making process was strictly controlled to minimize scatter in the test results. The beams and characterization specimens were cast at a mixing plant in Santhià, close to Turin.

The tests presented in this paper are part of a much larger investigation on plain and steel fiber RC beams. The determination of the fracture toughness and energy was accomplished according to the RILEM recommendation TC-89 procedure.[14] For the sake of comparison to the fiber-reinforced samples (not examined in this paper), however, the fracture energy was determined from the area underneath the loading curve, following the procedure proposed by Elices et al.,[15] Guinea et al,[16] and Planas et al.,[17] and the toughness evaluated by the relation $K_{IC} = \sqrt{G_F E}$, where G_F and E are the fracture energy and Young's modulus, respectively. The concrete compressive strength f_{ck} was measured on 5.9 x 5.9 x 5.9 in. (150 x 150 x 150 mm) cubic specimens, whereas the elastic modulus was measured on 3.9 x 3.9 x 11.8 in. (100 x 100 x 300 mm) specimens. The cylindrical strength f_c was obtained from the strength measured on the cubes by the formula $f_c = 0.85 f_{ck}$. The mean measured steel and concrete mechanical properties, as well as the standard deviations, are reported in Table 1.

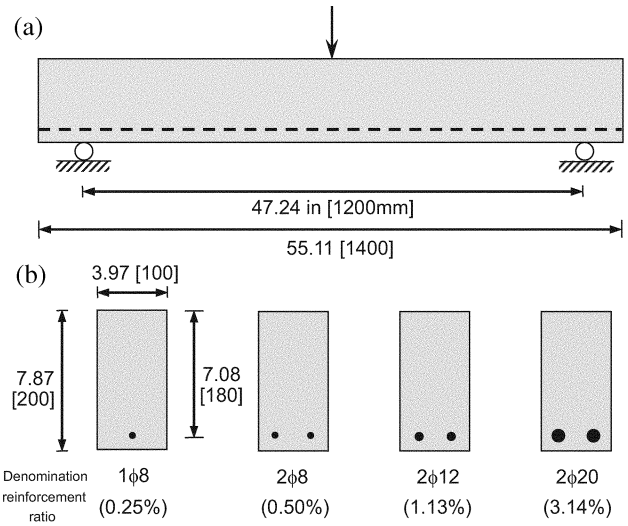

Fig. 1—Specimens' geometry. (Note: Dimensions in inches [mm].)

Table 1—Mechanical properties and standard deviations of steel bars and concrete

Steel bars	f_y, psi (MPa)	Standard deviation	f_k, psi (MPa)	Standard deviation	—	—
ϕ8	70,231 (484)	2662 (18)	91,332 (630)	3248 (22)	—	—
ϕ12	82,902 (572)	1317 (9)	93,686 (646)	232 (2)	—	—
ϕ20	72,982 (503)	351 (2)	90,658 (625)	240 (2)	—	—
Concrete	f_c, psi (MPa)	Standard deviation	E, psi (MPa)	Standard deviation	G_F, lb/in. (N/m)	Standard deviation
	5330 (36.75)	1078 (7.44)	4.795×10^6 (33,058)	1.218×10^5 (840)	0.587 (111.5)	5.4×10^{-2} (10.33)

TESTING PROCEDURE

The test setup for all beam specimens was three-point bending, as illustrated in Fig. 1. A closed-loop servo-hydraulic dynamic testing machine with a capacity of 56 kip (250 kN) was used. The load was applied on a 1.97 in. (50 mm) wide steel plate at the midspan, equipped with two linear potentiometer transducers (LPTs) with a calibrated range of 3.93 in. (100 mm). The mean of the two readings was used to measure the vertical midspan deflection δ. Additional 1.97 in. (50 mm) range LPTs were placed at the supports for compensating the rigid body translations of the specimens.

The midspan deflection was chosen as the control parameter in the tests. The deflection rate was kept constant for all tests with a speed of 3.14×10^{-4} in.·s (8 μms^{-1}). The peak load was achieved for each specimen within approximately 15 to 20 minutes, depending on the reinforcement ratio. Each complete test had a duration of 30 to 45 minutes. The load F and the deflection under the load point δ were continually monitored and recorded. Finally, to complete the experimental data, the crack pattern on both sides of each specimen was acquired by high-resolution digital photographs. Four specimens were tested for each reinforcement percentage.

EXPERIMENTAL RESULTS

All the experimental load-versus-deflection curves (F-δ) for the RC beams are plotted in Fig. 2. To facilitate the

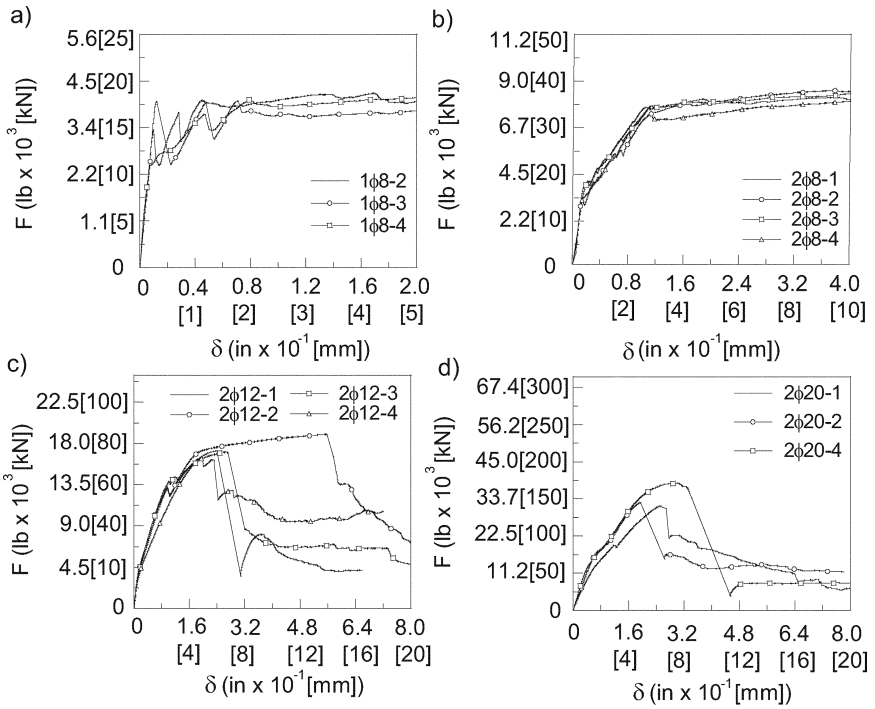

*Fig. 2—Experimental load-displacement (*F-δ*) curves.*

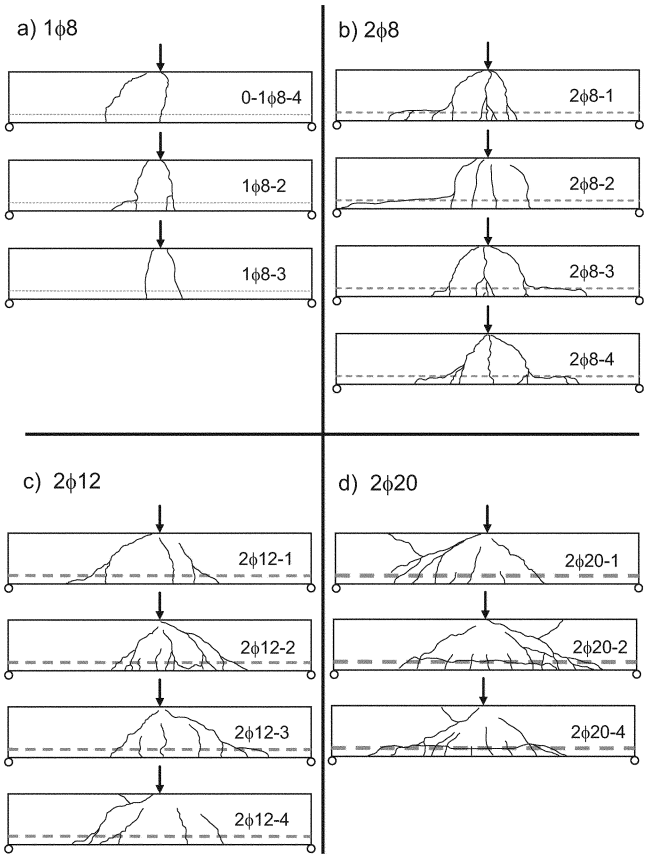

Fig. 3—Observed crack patterns.

comparison between curves corresponding to the same kind of beams, the initial slope of the curves is corrected to the theoretical value obtained from linear elastic calculations. The experimental initial slopes in an F-δ curve are usually different for the same kind of beam and the same setup. This is due to the sensitivity of the elastic flexibility of the beam to the boundary conditions in the application of a concentrated load.[17] An instrumentation error caused a load control failure for two samples, so data for 14 tests out of 16 samples are available, as reported in Fig. 2.

The behavior of the beams is almost linear up to the cracking load. For the beams with the lowest reinforcement ratios, the cracking load almost coincides with the ultimate load. As the reinforcement ratio increases, a change in the initial slope appears. Depending on the reinforcement ratio, two different behaviors after the cracking load are observed. In the case of the reinforcement ratios 0.25 and 0.50%, the reinforcement yields and the load remains approximately constant with increasing deflection and ductile failure. For beams with reinforcement ratios of 1.13 and 3.14%, a sudden decrease in the loading capacity is measured with no steel yielding and a brittle crushing failure mode. Note, incidentally, that Sample 2ϕ12*c* has a larger deflection at collapse because the crack pattern has a wider spread, as is apparent from Fig. 3.

The crack pattern is highly influenced by the reinforcement percentage, as shown in Fig. 3, where only one side of the specimen is reported. During the loading process, the first flexural cracks appear randomly distributed close to the midspan cross section. For the lowest reinforcement percentage (0.25%) (Fig. 3(a)), the steel yields very early in a crack and the overall cracking pattern is very limited. For beams with a 0.50% reinforcement percentage (Fig. 3(b)), the extension of the cracking area along the span increases, although the mechanical beam behavior is rather similar to the previous case: the steel yields at one of the cracks and the beam presents a ductile failure. Some horizontal cracks appear at the reinforcement level after steel yielding. These kinds of cracks are due to the combined effect of a dowel mechanism and the increased splitting stresses, but the beam loading capacity is not increased significantly due to the absence of stirrups. In

beams with a reinforcement percentage of 1.13% (Fig. 3(c)), flexural and shear-flexural cracks appear along the span. Compared to the previous cases, the crack pattern has a wider spread on the beam side. Failure is generated by an unstable crack growth process[12]; the reinforcing steel bars do not exhibit yielding; and a sudden, brittle collapse takes place (Fig. 2(c)). During the unstable crack growth, a redistribution of the shear carrying capacity from the concrete ligament to the steel bars occurs and a longitudinal crack starts at the reinforcement level. Finally, for the beams with the highest reinforcement ratio of 3.14% (refer to Fig. 3(d)), the most extended crack pattern is observed. Flexural and flexural-shear cracks appear along the span and the cracking process develops until a concrete crushing failure occurs, characterized by the typical wedge-shaped crack near the load application point.

In the next sections, the experimental results will be analyzed in light of the bridged crack model.[1,13,18] In this model, the nondimensional shear V_F at failure is governed by two brittleness numbers N_P and N_C

$$\tilde{V}_F = \frac{V_F}{K_{IC} h^{1/2} b}; \qquad N_P = \frac{f_y h^{1/2}}{K_{IC}} \rho; \qquad N_C = \frac{f_c h^{1/2}}{K_{IC}} \quad (1)$$

where K_{IC} is the concrete fracture toughness, f_y is the steel yielding strength, and f_c is the concrete crushing strength. Note that because the model is completely nondimensional, the sensitivity of the results to the mechanical material properties can be immediately observed from Eq. (1). In the three-point bending tests, the failure usually develops by forming a series of shear-flexural cracks along the shear span.

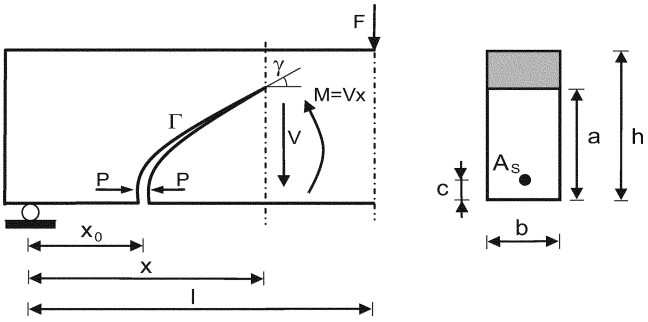

Fig. 4—Theoretical model problem.

At the beginning, the cracks follow a vertical trajectory and then turn toward the loading point. Although the cracking pattern in RC beams can be rather diffuse, especially with high reinforcement percentages, attention will be focused on the crack whose opening determines the final failure of the beam, referred to in the following as the critical crack. The experimental critical crack will be interpolated with an assumed crack shape for simulation purposes by the bridged crack model.[1,13,18] The assumed typical crack path is shown in Fig. 4, where some geometrical quantities used in the following developments are defined. The critical crack trajectory Γ is assumed as given by two parts. The first part Γ_1 is vertical and extends from the intrados to the reinforcement layer. The second part Γ_2 is assumed to be a power law with some given exponent, extending from the end of the first part to the loading point. Let h be the beam depth, l the shear span, a the crack depth, c the reinforcement cover, x the crack tip horizontal coordinate, x_0 the crack mouth horizontal coordinate, and μ the exponent of the crack trajectory function, and define

$$\alpha_0 = \frac{x_0}{l}; \qquad \alpha = \frac{x}{l}; \qquad \xi = \frac{a}{h}; \qquad \zeta = \frac{c}{h}; \qquad \lambda_l = \frac{l}{h} \quad (2)$$

The nondimensional form of the crack trajectory is

$$\alpha(\zeta, \xi) = \begin{cases} \alpha_0 & \zeta \geq \xi \\ \alpha_0 + \left(\dfrac{\xi - \zeta}{1 - \zeta}\right)^{\mu} (1 - \alpha_0) & \zeta \leq \xi \leq 1 \end{cases} \quad (3)$$

where α is the nondimensional horizontal distance of the crack tip from the support, ξ is the relative crack depth, α_0 is the crack mouth coordinate, and ζ is the reinforcement relative depth. All of these nondimensional parameters range between 0 and 1. Finally, λ_l is defined as the shear-span slenderness ratio $\lambda_l = l/h$.

Figure 5 shows the critical crack trajectories observed on each tested beam and reported in a nondimensional diagram. Half of the beam is represented. The arrow in each plot indicates the load application point and the support is at the abscissa $\alpha_0 = 0$.

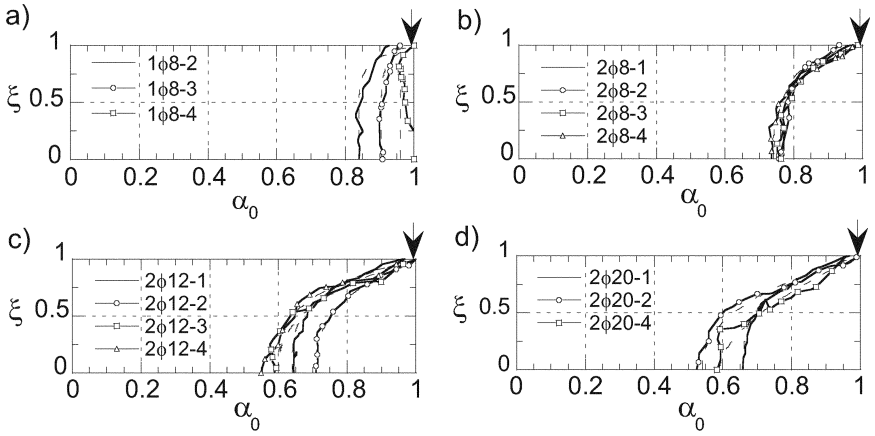

Fig. 5—Critical crack paths: (a) 1ϕ8; (b) 2ϕ8; (c) 2ϕ12; and (d) 2ϕ20.

Table 2—Parameters and model results for experimental program

Specimen	α_0	μ	$\tilde{V}_{test}^{*}$	Failure mode	N_P	N_C	$\tilde{V}$	ξ
1ϕ8-2	0.84	8.70	0.11	Flexural	—	—	—	—
1ϕ8-3	0.91	9.10	0.10	Flexural	—	—	—	—
1ϕ8-4	0.97	24.9	0.11	Flexural	—	—	—	—
1ϕ8-mean	0.91	14.2	0.11	Flexural	0.28	8.56	0.12	0.40
2ϕ8-1	0.77	5.29	0.22	Flexural	—	—	—	—
2ϕ8-2	0.78	6.05	0.23	Flexural	—	—	—	—
2ϕ8-3	0.76	3.76	0.24	Flexural	—	—	—	—
2ϕ8-4	0.74	3.21	0.22	Flexural	—	—	—	—
2ϕ8-mean	0.76	4.58	0.23	Flexural	0.57	8.56	0.21	0.62
2ϕ12-1	0.64	3.59	0.47	Shear	—	—	—	—
2ϕ12-2	0.72	2.74	0.52	Shear/flexural	—	—	—	—
2ϕ12-3	0.60	2.60	0.46	Shear	—	—	—	—
2ϕ12-4	0.61	3.30	0.45	Shear	—	—	—	—
2ϕ12-mean	0.64	3.06	0.47	Shear	1.51	8.56	0.44	0.53
2ϕ20-1	0.64	3.40	0.86	Shear/crushing	—	—	—	—
2ϕ20-2	0.54	2.32	0.90	Shear/crushing	—	—	—	—
2ϕ20-4	0.58	1.78	1.06	Shear/crushing	—	—	—	—
2ϕ20-mean	0.59	2.50	0.94	Shear/crushing	3.68	8.56	0.77	0.41

*Experimental failure nondimensional shear.

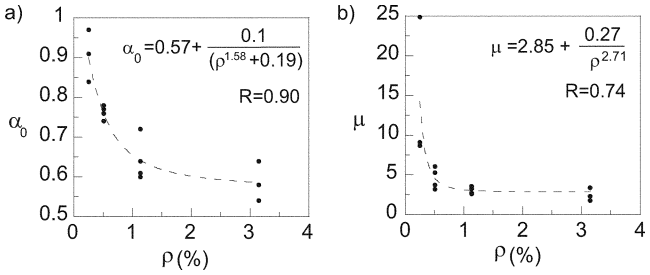

Fig. 6—Influence of reinforcement ratio ρ on critical crack trajectory parameters: (a) crack initiation point coordinate α_0; and (b) crack trajectory exponent μ.

From each test result, a nonlinear regression was performed to obtain the nondimensional parameters α_0 and μ defining the crack trajectory (Eq. (5)). The results, including the sample designation, the nondimensional failure shear $\tilde{V}_{test}$, and the failure mode are reported in the first five columns of Table 2.

Figure 6(a) analyzes the influence of the reinforcement ratio ρ on the nondimensional critical crack mouth position α_0. The dashed line plots the nonlinear data regression with the following law.

$$\alpha_0 = 0.57 + \frac{0.10}{0.19 + \rho^{1.58}} \quad (4)$$

As the reinforcement ratio increases, the value of α_0 decreases—that is, the critical crack originates closer to the support. It can be observed that, when the reinforcement ratio increases, the initiation point of the critical crack approaches the value $\alpha_0 \cong 0.50$—that is, the critical crack develops near the central part of the shear span. Equation (4) is useful to provide the critical crack initiation point α_0, which can be compared to the one predicted by the model proposed in the first part of the present work.[1]

The crack path exponent μ has been defined in this paper by nonlinear regression of the digitized crack trajectories with regard to the sample reinforcement, assuming a law that best fitted the experimental results (Fig. 6(b)). The exponent tends to be smaller as the reinforcement ratio increases. This is a consequence of a smaller inclination of the critical crack with respect to the beam axis as the reinforcement percentage increases. The dashed line shown in Fig. 6(b) is the nonlinear regression curve showing the following data trend.

$$\mu = 2.85 + \frac{0.27}{\rho^{2.71}} \quad (5)$$

The experimental data nonlinear regressions (Eq. (4) and (5)), as well as the used geometrical and material data together with the collapse loads, are of primary importance in the validation of theoretical models—for example, the bridged crack model considered in this paper or the strut-and-tie formulation.[19] Of course, the validity of Eq. (4) and (5) is limited to the extent considered in the experimental program and does not include important parameters like the shear-span slenderness ratio λ_l.

BRIDGED CRACK MODEL

The results of the experimental tests have been used for an experimental validation of the bridged crack model,[1,13,18] briefly recalled herein.

In the model, it is assumed that the crack propagates only in Mode I. The crack propagation condition is ruled by the comparison of the stress-intensity factor K_I (Eq. (6)), with the concrete fracture toughness K_{IC}

$$K_I = K_{IV} - K_{IP} = K_{IC} \quad (6)$$

where K_{IV} is the stress-intensity factor due to the external load, and K_{IP} is the stress-intensity factor due to the closing forces applied by the reinforcement bars. An approximate

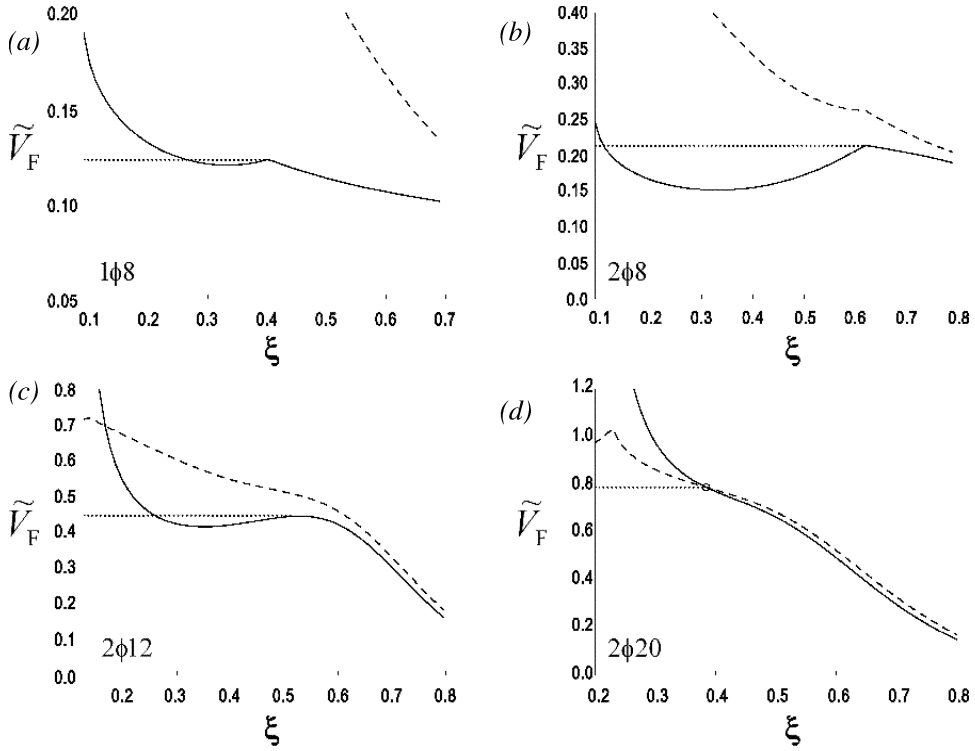

Fig. 7—Failure shear model prediction: (a) 1ϕ8; (b) 2ϕ8; (c) 2ϕ12; and (d) 2ϕ20. Solid curve is $\tilde{V}_F$*; dashed curve is* $\tilde{V}_C$.

analytical expression for the stress-intensity factors is introduced. This assumption has been validated by computing the stress-intensity factors numerically through the boundary element code developed by Portela and Aliabadi.[20] The relative displacement in the cracked cross section at the level of reinforcement is assumed to be equal to zero up to the yielding or slippage of the reinforcement; this compatibility condition allows the reinforcement reaction to be obtained. When the starting point abscissa of the crack trajectory is at the beam midspan, the model naturally coincides with the traditional bridged crack model[21,22] introduced for the pure flexural problem.

Concrete crushing is then analyzed by evaluating the compressive stress in the upper part of the beam. The basic concept is to express the stress state at the upper edge of the cracked section as the sum of the contribution σ_c^V due to shear (that is, to the bending moment at the cross section containing the crack tip) and the contribution σ_c^P due to the reinforcement reaction

$$\sigma_c = \sigma_c^V + \sigma_c^P \tag{7}$$

Concrete crushing can be detected by comparing the stress σ_c to the crushing strength f_c, which is a material property. The crushing shear V_C can be found by intersecting the crushing curve obtained from Eq. (7) with the crack propagation curve given by Eq. (6). In this way, the equilibrium and compatibility equations are satisfied. A strain-based criterion could be defined as well, following the reasoning path outlined in the first part of the present paper.[1]

In the bridged crack model extension, the different collapse modes are joined together into a unified general framework so that the simulation of the transitional phenomena is easily accomplished. The detailed development of the theoretical model has been previously presented.[1,13,18]

COMPARISON BETWEEN MODEL RESPONSES AND TEST RESULTS

The results of the experimental program cover flexural, shear, and compression failures. The proposed computational model requires a few parameters, namely the materials' mechanical properties and the crack trajectory exponent, being able to predict the failure mode, the crack initiation point, and the failure load.

Therefore, the numerical simulations were carried out using the crack trajectory exponent determined from the analysis and reported in the second column of Table 2.

The model and experimental results are summarized in Table 2. The first four columns report the specimen label and the experimental data: the observed crack initiation point, the crack path exponent, the failure shear, and the observed and computed failure mode (they are coincident). The last four columns report the model data given by the brittleness numbers N_P *and* N_C, the computed failure shear V, and the crack depth at failure ξ.

In this section, the experimental failure crack data—that is, the starting point and the crack shape—are put into the model and the failure load and collapse mode are evaluated and compared to the experimental data. Figure 7 shows the plots of the nondimensional crack propagation shear V_F (solid curves) and the concrete crushing shear V_C (dashed curves) versus crack depth. The horizontal dotted line shows the computed failure shear.

The parameters introduced into the model were obtained from the material characterization tests. The critical crack trajectory is determined from the mean of the experimental data. The relevant data are summarized in Tables 1 and 2.

As pointed out in the first part of the present work,[1] the crack propagation process may present stable or unstable behavior. When the crack growth is stable, an increase in the crack depth requires a load increase to fulfill the model equations. On the contrary, unstable crack growth requires a load decrease. Both kinds of behavior can occur during crack propagation (refer to Fig. 7).

For the beams labeled 1ϕ8 (reinforced with a single 0.315 in. [8 mm] diameter bar), the critical crack initial position is observed close to the midspan ($\alpha_0 \cong 1.0$). Immediately after the crack path crosses the reinforcement ($\xi > 0.1$), an unstable branch begins. This turns out to be stable for a crack depth $\xi \cong 0.3$. Then, the nondimensional shear force increases until the yielding of steel takes place ($\xi \cong 0.4$). The reinforcement reaction stabilizes the initially unstable crack propagation up to steel yielding (Fig. 7(a)). Therefore, the beam failure mode is flexural with a model nondimensional failure shear of 0.12, very close to the experimental results.

The second plot (Fig. 7(b)) shows the results for the beams with a reinforcement ratio of 0.5%, labeled 2ϕ8. These beams are reinforced with two 0.315 in. (8 mm) diameter bars. The results show a behavior similar to that of the previous 1ϕ8 beams. The nondimensional shear at failure increases due to the increase in the reinforcement percentage. A stable branch follows the initial unstable one and the crack grows until it reaches steel yielding at $\xi = 0.6$. The cracking zone at failure is wider and located farther from the midspan than in the previous case ($\alpha_0 = 0.76$; refer to Table 2). The beam failure mode is again flexural with a model nondimensional failure shear of 0.21—in good agreement with the experimental results.

Figure 7(c) shows the results for beams labeled 2ϕ12 and reinforced with two 0.472 in. (12 mm) diameter bars. The behavior for low values of the crack depth is similar to the previous cases. The stable branch reaches a maximum at $\xi \cong 0.55$, then the type of propagation changes and an unstable crack growth leads to failure. This change in the nature of crack propagation for a shear crack in RC beams without stirrups has been reported experimentally by Carmona et al.[12] The failure crack is closer to the central part of the shear span ($\alpha_0 = 0.64$), as also pointed out experimentally by Kim and White,[23,24] who observed that the shear failure occurs when the crack tip is close to the ideal line joining the support with the point of load application and the crack inclination at the crack tip is almost parallel to this line. The model results show a change in the trend of the crack propagation curve: steel yielding is not observed, and the model failure load is given by the maximum of the crack propagation curve, as discussed in Part 1 of the present work.[1] The failure mode changes to shear and the predicted nondimensional failure shear is 0.44, slightly lower than the test results.

Note that, after the maximum load and during the unstable crack growth, a redistribution of the shear carrying capacity occurs from the concrete ligament to the steel bars and then a longitudinal crack at the reinforcement level forms and propagates. This secondary effect after the maximum load is outside the capability of the present model.

Finally, Fig. 7(d) represents the results for the beams with the highest of the examined reinforcement ratios (3.14%), labeled 2ϕ20 and reinforced with two 0.787 in. (20 mm) diameter bars. The crack initiation point shifts more toward the supports ($\alpha_0 = 0.59$); a typical wedge expulsion is observed in the uppermost part of the beam. The model crack propagation curve intersects the crushing curve, detecting failure by concrete crushing. The predicted failure nondimensional shear is 0.77, approximately 18% lower than the experimental value.

In conclusion, the model correctly predicts the experimental failure mode transition by increasing the reinforcement ratio (yielding $\rightarrow$ shear $\rightarrow$ crushing) according to the global transition scheme.[1,18] The least accurate prediction concerns the crushing failure where, as pointed out in the first part of the present work,[1] a strain-based criterion may be introduced to account for concrete nonlinearity. This topic is currently under development.

CONCLUSIONS

This paper presents recent experimental results on RC beams without stirrups. The program was designed to study the influence of the reinforcement ratio on the crack pattern and the ductile-to-brittle failure transition in RC beams. An extensive analysis of the initial location and shape of the critical crack—that is, the crack driving the beam collapse—and of its relation to the failure mode was performed. The experimental results are analyzed with the help of an extension of the bridged crack model.[1,13,18] The model is able to analyze the progress of flexural-shear cracks detecting the failure mode (flexural, shear, or compression) within a unified framework. The following conclusions can be drawn from this study:

1. The crack pattern and the mechanical behavior observed in an RC beam are very sensitive to the amount of reinforcement. The crack pattern in the element—that is, the initial position and shape of the cracks—will depend on the reinforcement ratio. The cracks will propagate toward the load application point and one of them, herein called the critical crack, provokes the failure of the element. This remark implies a direct relation between the cracking process and the failure mode.

2. Cracks near the midspan are associated with flexural failure and have a stable growth process, whereas cracks in the central part of the shear span are associated with shear failure. The extension and trajectory of the critical crack are controlled by the reinforcement ratio and the failure mode.

3. The theoretical model and the experimental evidence show that shear failure is due to an unstable crack growth from flexural-shear cracks. Whereas the reinforcement reaction stabilizes the propagation of flexural cracks, a point where the reinforcement cannot control the propagation is observed in shear cracks, so that the propagation turns out to be unstable, leading the beam to collapse.

ACKNOWLEDGMENTS

J. R. Carmona gratefully acknowledges financial support for this research provided by the Junta de Comunidades de Castilla-La Mancha under Grant No. PAI08-0196-8210.

A particular acknowledgment goes to Buzzi-Unicem and E. Moretti for their full support and cooperation in preparing all the samples and their transportation to the Fracture Mechanics Laboratory of the Politecnico di Torino. Financial support from the Italian Ministry of Scientific Research under Programs PRIN 2004, 2005, and 2008 is also acknowledged.

NOTATION

A_s = reinforcement area
a = crack depth
b = beam width
c = reinforcement cover
E = concrete Young's modulus
F = applied load
f_c = concrete crushing strength

f_{tt} = ultimate steel reinforcement stress
f_y = steel reinforcement yielding stress
G_F = concrete fracture energy
h = beam depth
K_{IC} = concrete toughness
K_{IP} = stress-intensity factor due to closing force at reinforcement
K_{IV} = stress-intensity factor associated with shear force
l = shear span
N_C = brittleness number (crushing)
N_P = brittleness number (bending)
V_C = shear of crushing failure
V_F = shear of crack propagation
$\underline{V}_C$ = nondimensional shear of crushing failure
$\underline{V}_F$ = nondimensional shear of crack propagation
V_{test} = maximum measured nondimensional shear from beam specimen test
x = crack tip horizontal position
x_0 = crack mouth horizontal position
α = nondimensional horizontal distance from support to crack tip
α_0 = nondimensional initial crack mouth position
δ = vertical deflection under load point
λ_l = shear-span slenderness ratio
μ = trajectory exponent
ρ = reinforcement ratio
σ_{c_P} = stress at beam midspan, uppermost point
σ_c^P = stress at beam midspan, uppermost point, due to reinforcement reaction
σ_c^V = stress at beam midspan, uppermost point, due to support reaction
ξ = nondimensional crack depth
ζ = nondimensional reinforcement cover

REFERENCES

1. Carpinteri, A.; Carmona, J. R.; and Ventura, G., "Failure Mode Transitions in Reinforced Concrete Beams—Part 1: Theoretical Model," *ACI Structural Journal*, V. 108, No. 3, May-June 2011, pp. 277-285.

2. Bosco, C.; Carpinteri, A.; and Debernardi, P. G., "Fracture of Reinforced Concrete: Scale Effect and Snap-Back Instability," *Engineering Fracture Mechanics*, V. 35, No. 4-5, 1990, pp. 228-236.

3. Bosco, C.; Carpinteri, A.; and Debernardi, P. G., "Minimum Reinforcement in High-Strength Concrete," *Journal of Structural Engineering*, ASCE, V. 116, No. 2, 1990, pp. 228-236.

4. Baluch, M. H.; Azad, A. K.; and Ashwavi, W., "Fracture Mechanics Application to Reinforced Concrete Members in Flexure," *Application of Fracture Mechanics to Reinforced Concrete*, A. Carpinteri, ed., Elsevier, London, UK, 1992, pp. 413-436.

5. Ulfkjaer, J. P.; Hededal, O.; Kroon, I.; and Brincker, R., "Simple Application of Fictitious Crack Model," *Size Effect in Concrete Structures*, H. Mihashi, H. Okamura, and Z. P. Bažant, eds., E&FN Spon, London, UK, 1994, pp. 281-292.

6. Hededal, O., and Kroon, I. B., "Lightly Reinforced High-Strength Concrete," master's thesis, University of Åalborg, Åalborg, Denmark, 1991, 88 pp.

7. Carpinteri, A., "Minimum Reinforcement in Concrete Members," *ESIS Publications*, V. 24, Elsevier, London, UK, 1999, 30 pp.

8. Ruiz, G.; Elices, M.; and Planas, J., "Experimental Study of Fracture of Lightly Reinforced Concrete Beams," *Materials and Structures*, V. 31, 1998, pp. 683-691.

9. Ruiz, G., and Carmona, J. R., "Experimental Study on the Influence of the Shape of the Cross-Section and of the Rebar Arrangement on the Fracture of Lightly Reinforced Beams," *Materials and Structures*, V. 39, 2006, pp. 343-352.

10. Karihaloo, B., *Fracture Mechanics & Structural Concrete*, Longman Scientific & Technical, New York, 1995, 330 pp.

11. Gustafsson, P. J., "Fracture Mechanics Study of Non-Yielding Materials Like Concrete: Modeling of Tensile Fracture and Applied Strength Analyses," *Report* No. TVBM-1007, Division of Buildings Materials, Lund Institute of Technology, Lund, Sweden, 1985.

12. Carmona, J. R.; Ruiz, G.; and del Viso, J. R., "Mixed-Mode Crack Propagation through Reinforced Concrete," *Engineering Fracture Mechanics*, V. 74, 2007, pp. 2788-2809.

13. Carpinteri, A.; Carmona, J. R.; and Ventura, G., "Propagation of Flexural and Shear Cracks through Reinforced Concrete Beams by the Bridged Crack Model," *Magazine of Concrete Research*, V. 59, No. 10, 2007, pp. 743-756.

14. RILEM TC 89-FMT, "Determination of Fracture Parameters of Plain Concrete Using Three Point Bend Tests," *Materials and Structures*, V. 23, 1990, pp. 457-460.

15. Elices, M.; Guinea, G. V.; and Planas, J., "Measurement of the Fracture Energy Using Three-Point Bend Tests—Part 3: Influence of Cutting the *P*-δ Tail," *Materials and Structures*, V. 25, 1992, pp. 327-334.

16. Guinea, G. V.; Planas, J.; and Elices, M., "Measurement of the Fracture Energy Using Three-Point Bend Tests—Part 1: Influence of Experimental Procedures," *Materials and Structures*, V. 25, 1992, pp. 121-128.

17. Planas, J.; Guinea, G. V.; and Elices, M., "Stiffness Associated with Quasi-Concentrate Loads," *Materials and Structures*, V. 27, 1992, pp. 311-318.

18. Carpinteri, A.; Carmona, J. R.; and Ventura, G., "Flexural to Shear and Crushing Failure Transitions in RC Beams by the Bridged Crack Model," *Fracture Mechanics of Concrete Structures*, Proceedings of the VI International FraMCoS Conference, Catania, Italy, 17-22 June 2007, Taylor & Francis, London, UK, 2007, pp. 677-684.

19. Schlaich, J.; Schafer, K.; and Jennewein, M., "Toward a Consistent Design of Structural Concrete," *PCI Journal*, V. 32, No. 3, 1987, pp. 74-150.

20. Portela, A., and Aliabadi, M. H., "Crack Growth Analysis Using Boundary Elements," *Computational Mechanics Publications*, Southampton, UK, 1992, 50 pp.

21. Carpinteri, A., "A Fracture Mechanics Model for Reinforced Concrete Collapse," *Proceedings of the I.A.B.S.E. Colloquium on Advanced Mechanics of Reinforced Concrete*, Delft, the Netherlands, 1981, pp. 17-30.

22. Carpinteri, A., "Stability of Fracturing Process in RC Beams," *Journal of Structural Engineering*, ASCE, V. 110, 1984, pp. 544-558.

23. Kim, W., and White, R. N., "Shear-Critical Cracking in Slender Reinforced Concrete Beams," *ACI Structural Journal*, V. 96, No. 5, Sept.-Oct. 1999, pp. 757-765.

24. Kim, W., and White, R. N., "Hypothesis for Localized Horizontal Shearing Failure Mechanism of Slender RC Beams," *Journal of Structural Engineering*, ASCE, V. 125, No, 10, 1999, pp. 1126-1135.